Journal of Materials Science: Materials in Electronics
https://doi.org/10.1007/s10854-018-0404-3

Integral nanoindentation evaluation of TiO_2, SnO_2, and ZnO thin films deposited via spray-pyrolysis on glass substrates

Edgar A. Villegas[1] · Rodrigo Parra[1] · Leandro Ramajo[1]

Received: 13 July 2018 / Accepted: 16 November 2018

Abstract
Tin, titanium and zinc oxide thin films were deposited on glass substrates by spray-pyrolysis. According to the resolution of XRD and SEM, films are single phase and of uniform surfaces. Elastic modulus and film hardness were studied by instrumented indentation. Friction coefficient and wear volume were determined by nanowear procedures. Low friction coefficient and roughness (< 0.2 and ~ 7 nm, respectively) were measured. Hardness values (between 6 and 11 GPa) were determined to be in agreement with those reported for similar films grown by physical methods. Titanium and tin dioxide films displayed better wear and mechanical properties than ZnO films.

1 Introduction

Touch-screen, UV-light emitters, and electrochromic windows are some of the extended electronic applications of ceramic transparent thin films. Such products exploit the mechanical properties of transparent conductive oxides (TCO) to ensure patterning durability and accuracy [1–4]. However, to become potential candidates for these applications, thin films should exhibit high transparency, high conductivity, homogeneity, good adhesion, hardness and chemical stability under different environmental conditions.

Coatings made from tin, titanium or zinc oxides (SnO_2, TiO_2 and ZnO, respectively) are inexpensive to produce, nontoxic, easily doped and chemically stable. They have also a large band-gap, and when doped can show high conductivity and high excitation-binding energy [5–8]. Very often it is also desirable to join different (sometimes opposite) properties in one coating, that is, preparation of multifunctional coatings. Such coatings are widely used in many fields of science and technology. This concerns the functional optical coatings presenting additional properties as increased hardness, hydrophobicity or resistance to abrasion [5].

These films are grown by different techniques, such as magnetron sputtering, reactive evaporation, chemical vapor deposition (CVD), pulsed laser deposition (PLD) and spray-pyrolysis (SP), among others [9–12]. Spray-pyrolysis presents several advantages, such as simplicity and low cost of the equipment involved.

Concerning the mechanical properties, nanoindentation has been widely used to determine the elastic modulus and hardness of thin films [13–17]. In contrast to microindentation, nanoindentation does not require a separate measurement of the contact area. The penetration depth of the specimen during nanoindentation is related to the actual contact area via a calibrated indenter tip. This technique offers an approach to determine the elastic modulus and hardness of ultra-thin films, which is difficult to attain by other methods.

The mechanical properties of oxide films grown by spraying have been seldom reported in the literature [18]. In this work, TiO_2, SnO_2 and ZnO thin films deposited by spray-pyrolysis on glass substrates at 450 °C were characterized by nanoindenting techniques. Additionally, the influence of microstructure on mechanical properties and wear were studied, as well as surface morphology and optical properties. Hereafter, these properties are shown and discussed for thin transparent films grown by spraying.

✉ Edgar A. Villegas
evillegas@fi.mdp.edu.ar

✉ Leandro Ramajo
lramajo@fi.mdp.edu.ar

[1] Institute of Research in Materials Science and Technology (INTEMA), CONICET - National University of Mar del Plata, Av. Cristóbal Colón 10850, B7606BWV Mar del Plata, Argentina

Published online: 27 November 2018

2 Experimental procedure

2.1 Preparation process

Thin films of titanium, tin and zinc oxides, were deposited by spray-pyrolysis on 7 cm × 2.5 cm soda-lime substrates. Titanium isopropoxide, tin(II) 2-ethylhexanoate and zinc acetate were used as precursors. In every case, solutions were prepared in 20 ml of ethanol and acetylacetone was used in order to assist solubilization. The solutions were deposited on substrates, previously washed and dried, at 425 °C by spraying using N_2 at 1.5–2 bar as carrier gas. In order to avoid diffusion of sodium ions from the substrate to the film, substrates were previously coated with a silica (SiO_2) film, which was deposited by immersion in a TEOS sol followed by a heat treatment at 500 °C. Profilometry measurements were facilitated by the presence of a mask on the substrate during spraying. The mask leaves a regular step between coated and uncoated areas.

2.2 Microstructural characterization

Microstructures were evaluated by means of a Field Emission Scanning Electron Microscope (FEI QUANTA FEG 250). Crystalline phases were characterized by Grazing Incidence X-Ray Diffraction (PANalytical X´pert Pro, CuKα radiation) between 20 and 80° 2θ with a step size of 0.0334° and a recording time of 100 s. No filters were used under this configuration.

2.3 Optical and electrical characterization

Optical transmittance was measured on the basis of UV–Visible spectra registered with a UV-VIS-NIR Shimadzu 3600 spectrophotometer, equipped with an integrating sphere, in the 3600–200 nm range. The Van der Pauw method was applied to electrical measurements using a two Digital Multimeter Rigol DM 3062, applying a 30 V bias voltage.

2.4 Mechanical characterization

Elastic modulus and hardness were measured by means of a Hysitron Triboindenter. A Berkovich diamond indenter with a total included angle of 142.3° was used for every measurement of 20 load–unload cycles with 450 μN. The data sets were processed using appropriate software to produce load–displacement curves [19]. The Hertzian method [20, 21], which proposes the estimation of the slope of the unloading curve by first fitting the entire unloading data, was employed to determine the reduced (E_r) and the hardness (H) of the materials. The reduced elastic modulus is related to the elastic modulus of the sample (E) and the contact stiffness (S) by means of the following equations:

$$P = ah^{3}/2 \tag{1}$$

$$a = \left(\frac{4}{3} E_r \sqrt{R}\right) \tag{2}$$

$$\frac{1}{E_r} = \frac{\left(1-\upsilon^2\right)}{E} + \frac{\left(1-\upsilon_i^2\right)}{E_i} \tag{3}$$

$$E_r = S.\left(\frac{\pi}{4A_{max}}\right)^{1/2}, \tag{4}$$

where υ is the Poisson's ratio and subscript i denotes the indenter material, R represents the indenter radius which is 25 nm, h is the displacement and P the force applied. Making a fitting to P–h curves, E_r is obtained.

A_{max} is the surface contact area at the maximum displacement. The contact stiffness (S) is the slope of the unloading curve taken as the first derivative in the maximum depth of a fitted power law function of the unloading segment of the curve. For the indenter tip used in this work, E_{iis} 1140 GPa and υ_{iis} 0.07, while the Poisson ratio was assumed to be 0.25.

The material hardness (H) was defined as the maximum load, P_{max}, divided by the projected area of the indentation under this load, Eq. (5):

$$H = \frac{P_{max}}{A_{max}} \tag{5}$$

The tip area function $A(hc)$ was calibrated from indentations upon a fused silica sample of known E.

2.5 Frictional behavior

The Hysitron Triboindenter was also used for nanoscratch tests. The load was ramped from 0 to 450 μN in 30 s, and the scratch length was set as 1500 μm at a moving velocity of 50 μm/s. Scanning wear tests were performed on each sample using a diamond cube-corner probe. Each test consisted of 25 cycles with a scan size of 20 μm. Wear tests were performed at normal loads of 200 μN on each sample. After wear tests were completed, the areas were imaged using a 60 μm scan size. These images were then analyzed to determine whether film failure had occurred. Also, Scanning Probe Microscopy (SPM) analyses, using Gwyddion Software was used.

3 Results and discussion

Figure 1 shows the XRD patterns of TiO_2, SnO_2 and ZnO films deposited by spray-pyrolysis on glass substrates at 450 °C. The patterns show the diffraction peaks of TiO_2 (JCPDS 01-083-2243), SnO_2 (JCPDS 077-0451) and ZnO (JCPDS 01-075-0576), indicating no preferred crystalline orientation in the films. Diffraction peaks due to the K_β line of Cu are observed, and identified, in patterns of TiO_2 and ZnO.

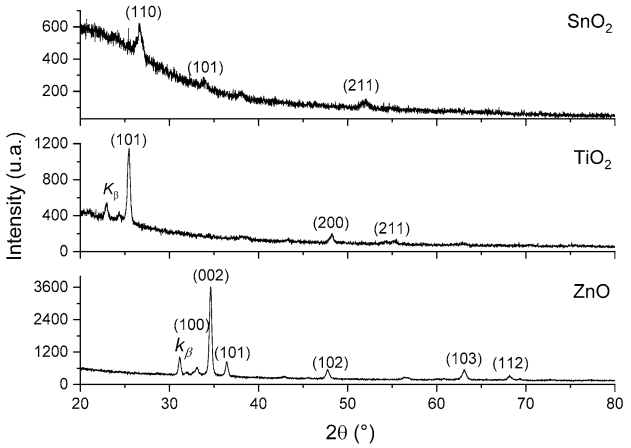

Fig. 1 XRD patterns of TiO_2, SnO_2 and ZnO thin films deposited by spray-pyrolysis at 450 °C

FE-SEM images in Fig. 2 show dense films with uniform crack-free surfaces. Apparently, the SnO_2 film is composed of the smallest grains, whereas the ZnO film showed the biggest. In addition, from SPM analyses, films display very small surface roughness of only a few nanometers as shown in Table 1. Film thicknesses measured by profilometry revealed that SnO_2, TiO_2 and ZnO films are of similar thickness of about 400 nm. The regular thickness values and the low roughness obtained in all samples suggest that the spraying is a useful method to obtained good quality reproducible films.

Electric resistivity and refraction index of TiO_2, SnO_2, and ZnO thin films were measured and results are shown in Table 1. It can be observed that the films present high resistivity; while refractive index (n) values are similar to the usual values reported for these materials [22–25]. However, SnO_2 films showed the lower resistivity values. Non-stoichiometry is the reason for the low resistivity of SnO_2 [26]. In fact, the formation energy of oxygen vacancies in SnO_2 is very low, causing the natural nonstoichiometry and

Table 1 Thickness (d), average roughness (R_a), electrical resistivity (σ) and refraction index (n) of TiO_2, SnO_2, and ZnO thin films

Film	d (nm)	R_a (nm)	σ (Ω cm)	n
TiO_2	446	5.70	∞	2.58
SnO_2	189	6.36	378	1.78
ZnO	527	7.96	1580	2.01

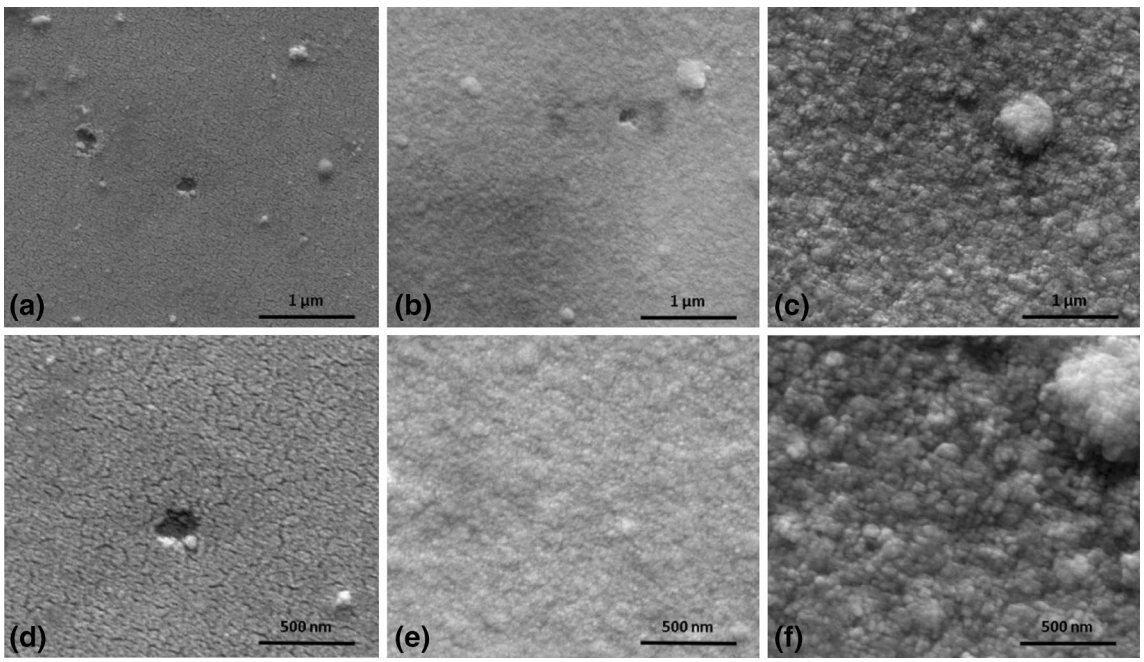

Fig. 2 SEM images of (**a**, **d**) SnO_2, (**b**, **e**) TiO_2, and (**c**, **f**) ZnO films. Scale bars 1 µm and 500 nm

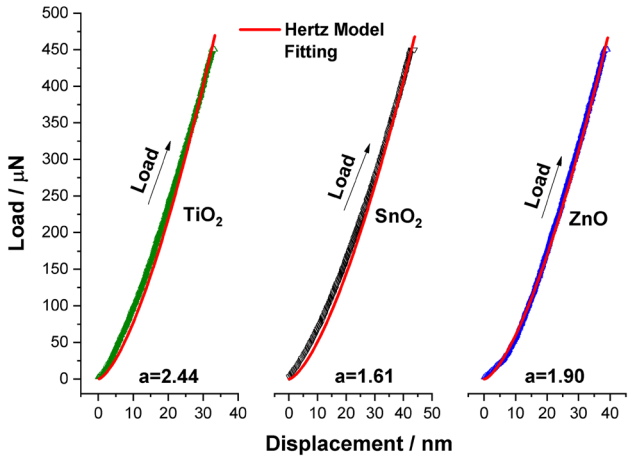

Fig. 3 Load-depth curves for films using a 450 µN load. Measured displacements were higher than 30 nm in either sample

Table 2 Average elastic modulus (*E*), hardness (*H*), friction coefficient (*Coef.*) and wear volume (*Vol.*) of films

Film	*E* (GPa)	*H* (GPa)	*Coef.*	*Vol.* (µm^3)	Reference
TiO_2	92.2 ± 4.1	10.7 ± 0.8	0.128	2.45	This work[a]
SnO_2	78.5 ± 0.4	6.1 ± 0.1	0.137	2.26	This work[a]
ZnO	108.2 ± 7.3	7.3 ± 0.8	0.178	7.68	This work[a]
TiO_2	161	9.4	–	–	[5]
SnO_2	71	5.1	–	–	[33]
ZnO	–	8	0.29	3	[34]
In-SnO_2	100	6.5	–	–	[31]
In-ZnO	140	10.6	–	–	[31]
CrN	–	23.4	–	–	[35, 36]
TiN	–	24	–	–	[37]

[a]Wear volume obtained after 15 cycles under a 200 µN load

the low resistivity observed in SnO_2 with respect to other semiconductors. Moreover, nominally undoped SnO_2 has a carrier density of up to 10^{20} cm^{-3} [27]. On the other hand, TiO_2 and ZnO present higher resistivities. Oxygen vacancies are deep donors in ZnO, being unlikely to cause *n*-type conductivity [28, 29].

Figure 3 shows load–displacement curves for TiO_2, SnO_2, and ZnO films. The parameter *a* from Eq. (2) is showed, and from these values the elastic modulus is calculated. Following the Hertzian model and approaching a fitting to *P*–*h* curves, different values of *a* can be calculate. All curves were approached to 3/2 power to fit with the Hertzian model.

Compared to other transparent oxides Table 2, the films showed good stiffness and hardness [30, 31]. The low scattering on elastic modulus and hardness data may be due to the low porosity and roughness Table 1. Although ZnO showed a relatively low mechanical performance compared to values reported by other researches [31, 32], this film displayed higher stiffness than TiO_2 and SnO_2 films, even though TiO_2 resulted harder.

The friction coefficients and wear volumes obtained by nanoindentation showed similar performances on TiO_2 and SnO_2 films related to ZnO. The three samples showed low friction coefficients (< 0.2) in agreement with previous reports [31, 32, 38], although ZnO clearly showed a lower performance. The wear behavior observed is strongly related to the friction behavior for each pair [32], which is related to the wear volume. In this way TiO_2 and SnO_2 showed lower values than ZnO, which is an indication that TiO_2 and SnO_2 actually protected the indentation point to a certain extent before damage occurred. This was expected as the average friction coefficients of these films were lower than that of ZnO-film. Then, shear stresses imposed on SnO_2 and TiO_2 coatings are reduced, leading to wear reduction. The higher roughness, grain size and thickness of the ZnO film are probably the reasons for its lower wear and mechanical performances with respect to SnO_2 and TiO_2 films.

The representative 60 µm, 2-D topographical in-situ SPM images of TiO_2, SnO_2 and ZnO surfaces, after 20 µm, 25 nanowear tests with 200 µN peak loads along the respective wear profile, are shown in Fig. 4. Images with associated wear forces showed no film failure, based on post-test Z-heights of 20 µm nanowear areas. Nanowear results on samples can be used to rank the best wear resistance analyzed film failure at each load. Using this ranking system, results in Table 2 show the ranking order for best wear resistance to be TiO_2, SnO_2, and ZnO, which is in agreement with SPM results. Although these are promising results, further studies are needed before using spraying for the deposition of protective oxide coatings for, e.g., opthalmics, automotive or flat panel display industry. Reference hardness values for tin, titanium and zinc oxide films are shown in Table 2 for the sake of comparison. Films of known "hard" materials such as CrN and TiN are also included [35–37]. It can be observed that the hardness values for TiO_2, SnO_2 and ZnO thin films measured in this work are comparable with those reported in the literature.

4 Conclusions

Tin, titanium and zinc oxide thin films deposited on glass substrates by spray-pyrolysis were evaluated by naoindenting techniques. Uniform dense films with average roughness around 6.5 nm were deposited. Titanium and tin oxide coatings showed better mechanical properties and wear performance than ZnO films. Hardness values between 10.7 and 6.11 GPa were measured for TiO_2, SnO_2 and ZnO, which are comparable to hardness values of these oxide films grown by other techniques. These results are a contribution to the

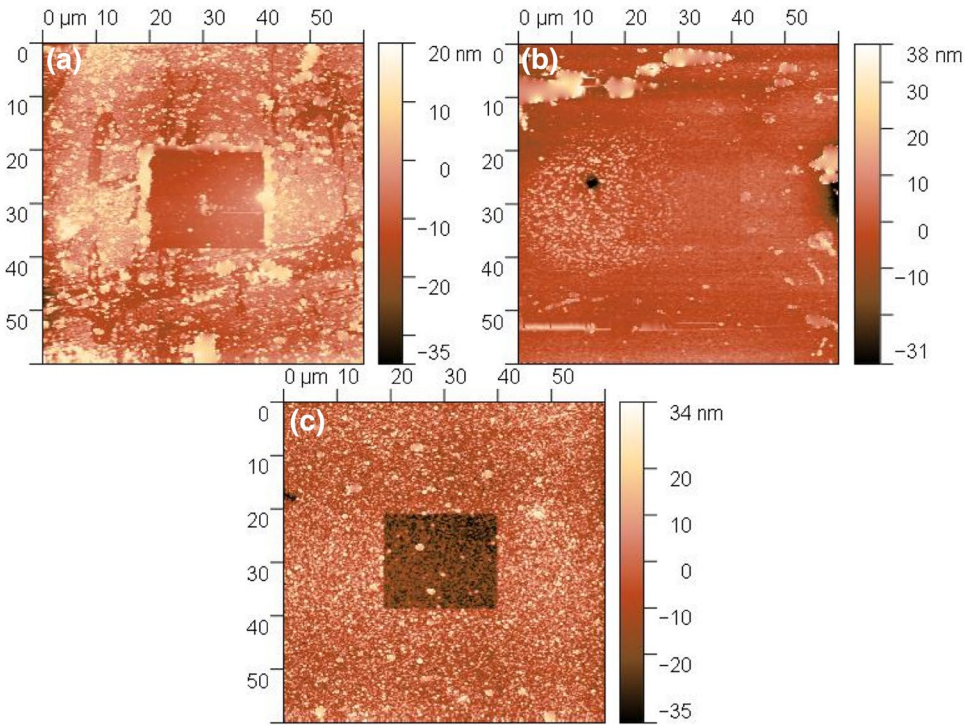

Fig. 4 60 µm, 2-D topographical in-situ SPM images of **a** TiO_2, **b** SnO_2 and **c** ZnO surfaces after nanowear tests (load 200 µN)

gap that exists on the reported mechanical properties of semiconducting-oxide films deposited by spray-pyrolysis.

Acknowledgements Thanks are due to V. Fuchs for XRD measurements, to M. Lere for equipment upgrade and design and B. Daga at the triboindenter lab. This work was carried out with the financial support of CONICET, ANPCyT (PICT'15 2305) and University of Mar del Plata.

References

1. M. Asghar, M. Shoaib, F. Placido, S. Naseem, Cent. Eur. J. Phys. **6**, 853–863 (2008)
2. M. Giotia, S. Logothetidis, C. Charitidis, Y. Panayiotatos, I. Varsano, Sens. Actuators A Phys. **99**, 35–40 (2002)
3. S.Y. Lien, D.S. Wuu, W.C. Yeh, J.C. Liu, Sol. Energy Mater. Sol. Cells **90**, 2710–2719 (2006)
4. J. Han, Y. Dou, M. Wei, D.G. Evans, X. Duan, Chem. Eng. J. **169**, 371–378 (2011)
5. M. Mazur, D. Wojcieszak, J. Domaradzki, D. Kaczmarek, S. Song, F. Placido, Opto-Electron. Rev. **21**(2), 233–238 (2013)
6. C. Martinet, V. Paillard, A. Gagnaire, J. Joseph, J. Non-Cryst. Solids **216**, 77–82 (1997)
7. N. Lehraki, M.S. Aida, S. Abed, N. Attaf, A. Attaf, M. Poulain, Curr. Appl. Phys. **12**, 1283–1287 (2012)
8. A. Ashour, M.A. Kaid, N.Z. El-Sayed, A.A. Ibrahim, Appl. Surf. Sci. **252**, 7844–7848 (2006)
9. C.Y. Tsay, C.W. Wu, C.M. Lei, F.S. Chen, C.K. Lin, Thin Solid Films **519**, 1516 (2010)
10. W.T. Yen, Y.C. Lin, P.C. Yao, J.H. Ke, Y.L. Chen, Thin Solid Films **518**, 3882 (2010)
11. H.J. Ko, Y.F. Chen, S.K. Hong, H. Wenisch, T. Yao, Appl. Phys. Lett. **77**, 3761 (2000)
12. A.R. Kaul, O.Y. Gorbenko, A.N. Botev, L.I. Burova, Superlattices Microstruct. **38**, 272 (2005)
13. A.C. Fischer-Cripps, Nanoindentation, (Springer, New York, 2004)
14. S.J. Bull, J. Phys. D Appl. Phys. **38**(25), R393 (2005)
15. S.Y. Chang, Y.C. Huang, Microelectron. Eng. **84**, 319 (2007)
16. J. Malzbender, J.M.J. den Toonder, A.R. Balkenende, Sci. Eng. R **36**, 47–103 (2002)
17. S.Y. Chang, H.L. Chang, Y.C. Lu, S.M. Jang, S.J. Lin, M.S. Liang, Thin Solid Films **460**, 164–167 (2004)
18. L. Filipovic, S. Selberherr, Sensors **15**, 7206–7227 (2015)
19. M.A. Ramírez, R. Parra, M.M. Reboredo, J.A. Varela, M.S. Castro, L. Ramajo, Mater. Lett. **64**, 1226–1228 (2010)
20. W.C. Oliver, G.M. Pharr, J. Mater. Res. **7**, 1564 (1992)
21. W.C. Oliver, G.M. Pharr, J. Mater. Res. **19**(1), 3–20 (2004)
22. S.H. Mohamed, J. Alloy. Compd. **510**, 119–124 (2012)
23. Y. Bouachiba, A. Bouvellou, F. Hanini, F. Kermiche, A. Taabouche, K. Boukheddaden, Mater. Sci. **32**(1), 1–6 (2014)
24. S. Sathish, B. Chandar Shekar, S. Chandru Kannan, R. Sengodan, K.P.B. Dinesh, R. Ranjithkumar, Int. J. Polym. Anal. Charact. **20**(1), 29–41 (2015)
25. R.M. Pasquarelli, D.S. Ginley, R. O'Hayre, Chem. Soc. Rev. **40**, 5406 (2011)
26. M. Batzill, U. Diebold, Surf. Sci. **79**, 47–154 (2005)
27. C. Kilic, A. Zunger, Phys. Rev. Lett. **88**, 095501 (2002)
28. M.D. McCluskey, S.J. Jokela, J. Appl. Phys. **106**, 071101 (2009)
29. K. Ellmer, J. Phys. D Appl. Phys. **34**, 3097–3108 (2001)
30. S.Y. Chang, Y.C. Hsiao, Y.C. Huang, Surf. Coat. Technol. **202**, 5416–5420 (2008)
31. K. Zeng, F. Zhu, J. Hu, L. Shen, K. Zhang, H. Gong, Thin Solid Films **443**, 60–65 (2003)
32. S.K. Wang, T.C. Lin, S.R. Jian, J.Y. Juang, J.S.C. Jang, J.Y. Tseng, Appl. Surf. Sci. **258**, 1261–1266 (2011)
33. T. Fang, W. Chang, Appl. Surf. Sci. **252**, 1863–1869 (2005)
34. S. Wanga, T. Lina, S. Jian, J. Juangb, J. Jangc, J. Tsengd, Appl. Surf. Sci. **258**, 1261–1266 (2011)

35. A. Zeilinger, R. Daniel, T. Schöberl, M. Stefenelli, B. Sartory, J. Keckes, C. Mitterer, Thin Solid Films **581**, 75–79 (2015)
36. P. Sukwisute, R. Sakdanuphab, A. Sakulkalavek, Mater. Today Proc. **4**, 6553–6561 (2017)
37. X. Feng, Y. Zhang, H. Hu, Y. Zheng, K. Zhang, H. Zhou, Appl. Surf. Sci. **422**, 266–272 (2017)
38. U.S. Mbamara, B. Olofinjana, O. Ajayi, C. Lorenzo-Martin, E.I. Obiajunwa, E.O.B. Ajayi, Eng. Sci. Technol. Int. J. **19**, 956–963 (2016)